ORIGINAL RESEARCH

An original donor-dependent spheroid system for the prediction of idiosyncratic drug-induced liver injury risk

Sara Cherradi[1] · Nicolas Taulet[1] · Hong Tuan Duong[1]

Abstract

One major drawback of preclinical models to test drug-induced liver injury (DILI) is their inability to predict the interindividual difference of DILI effect in a population. Consequently, a high number of molecules that passed preclinical phases, fail clinical trials, and many FDA-approved drugs were removed from the market due to idiosyncratic DILI. We use a proprietary-depleted human serum-based cell educating technology to generate donor-dependent spheroids with distinct morphology and functionality. We demonstrate that educated spheroids could capture the large variations in susceptibility to drug-induced liver injury between donors. We show that the model could predict clinical apparent DILI risk with a high specificity and sensitivity. We provide evidence that the model could address non-genetic factor-associated DILI risk and severity such as age or sex. Our study supports the benefit of using donor-dependent educated spheroids for hepatotoxicity evaluation in preclinical phase or in an exploratory study clinical trial phase 2 to provide a robust safety profile to a drug.

Introduction

The lack of sufficient compliance between preclinical models, including non-animal and animal models, and human physiology is a major cause of poor efficacy or of high toxicity of a drug when entering clinical trials [1, 2]. It is well accepted that people's susceptibility in drug responsiveness and drug-induced liver injury (DILI) is the main challenge in drug development and precision medicine [3, 4]. Nevertheless, it is currently impossible to test the interindividual variability of drug-mediated cellular responses before initiating clinical trials because of the lack of models that mimic that interindividual difference in a population [5]. Therefore, the generation of in vitro systems capable of mimicking cell functionality of human livers of a representative population to analyze drug-induced hepatotoxicity is necessary for the determination of safe medication dose ranges.

Because in normal physiological as well as in pathological conditions liver cells functions are not exclusively modulated by the intra-organ microenvironment but also by the inter-organ communication through plethora of released compounds including soluble factors, exosomes, and gut microbiota-derived metabolites and products that are found in the bloodstream [6–13], we developed a method that utilize depleted serum from each person to educate hepatic cell lines cultured as spheroids, to phenotypically mimic the interindividual difference in drug responsiveness.

We show that donor-dependent educated spheroids can predict clinical apparent DILI risk with a high specificity and sensitivity. Importantly, we demonstrate that our system could be used to assess non-genetic host factors such as age or sex that are linked to DILI risk and severity. To our knowledge, this is the first easy to set up human-derived model that better represents the variation of the human population making it a perfect tool to de-risk DILI for new compounds in development in pre-phase 1 or to provide a more robust safety profile to the drug in an exploratory study clinical trial phase 2.

Material and methods

Reagents, depleted serum, and cells

Blood samples are provided by the Etablissement Français du Sang (EFS) Hauts de France–Normandie. Depleted human

✉ Hong Tuan Duong
ht.duong@predictcan.com

1 PredictCan Biotechnologies SAS, Biopôle Euromédecine, Grabels, France

serum was obtained after a filtration step through a 0.45-µm mesh filter. The study was approved by the "Direction Générale de la recherche et de l'innovation" (CODECOH, n°DC-2021-4779). This project does not involve the human person according to the legislation (article L1121-1 du code de la santé publique). Albuterol, flavoxate, etoposide, β-estradiol, nizatidine, azathioprine, oxaliplatin, bosentan, sorafenib, cabozantinib, lenvatinib, rifampicin, and stavudine were purchased from CliniSciences (Nanterre, France). Hepatocyte (HepG2) and hepatic stellate cell lines (TWNT-1) were from ATCC (Molsheim, France) and Glow Biologics (Tarrytown, NY, USA), respectively. All cell culture reagents were provided by StemCell (Saint Égrève, France). Hepatocytes and hepatic stellate cells were conditioned for a minimum of 2 weeks in MammoCult® basal medium (StemCell) before use, to sensitize them to the cell educating technology. Absence of mycoplasma contamination was verified using MycoAlert® Mycoplasma Detection Kit from Lonza (Saint-Beauzire, France).

Generation of educated spheroids and treatments

Educated spheroids were generated from a co-culture of HepG2 and TWNT-1 cell lines in MammoCult® basal medium supplemented with depleted human serum for 3 days in 384 wells ultra-low attachment plates (Dutscher SAS, Bernolsheim, France). A dose-dependent treatment ranging from 0.01× to 100× C_{max} for each compound was performed for up to 96 h on educated spheroids. Cell viability was measured using CellTiterGlo (Promega, Charbonnières-les-Bains, France) according to the manufacturer's instructions.

Cytochrome P450 activity and total collagen type I quantification

CYP3A4 activity and total collagen deposition were assessed using P450-Glo™ CYP3A4 Assay (Promega, Charbonnières-les-Bains, France) and Total Collagen Assay Kit (Perchlorate-Free) (ab222942, Abcam, Paris, France) according to the manufacturer's instructions, respectively.

Immunofluorescence

Donor-dependent educated spheroids were cultured for 3 days in 96 wells ultra-low attachment plates (Dutscher, Bernolsheim, France). Spheroids were fixed with PBS-10% PFA (Fisher Scientific, Illkirch, France) for 30 min, permeabilized with PBS-0.5% Triton X-100 (Sigma-Aldrich, Saint-Quentin-Fallavier, France) for 2 h, and

incubated in blocking buffer (0.2% Triton X-100, Bovine Serum Albumin (Euromedex, Souffelweyersheim, France) in PBS) for 2 h at room temperature. Primary antibodies, including FITC-α-tubulin (F2168, Sigma-Aldrich), type 1 collagen (COL1A1, #72026, Cell Signaling, Ozyme, Saint-Cyr-L'École, France), Fibronectin (FN1, #26836, Cell signaling), FITC-α-smooth muscle Actin (ab8211, Abcam), ZO-1 (#61-7300, Life Technologies SAS, Courtaboeuf Cedex, France), and MRP2 (#4446, Cell Signaling) antibodies, were diluted in blocking buffer and incubated overnight at 4 °C. After washes with blocking buffer, the secondary antibody (anti-rabbit Alexa Fluor 555, #4413, Cell Signaling) was added for 3 h at room temperature followed by nuclei staining with DAPI (#4083, Cell Signaling). Spheroids were transferred into µ-Slide 8 Well (Ibidi, CliniSciences, Nanterre, France), and images were acquired on a Dragonfly spinning disk confocal microscope (Andor, Oxford Instruments, High Wycombe, UK) equipped with EMCCD iXon888 Life Andor camera (Objective 20X/0.75 NA) and controlled by Fusion software (Andor). Fluorescence intensity was quantified using ImageJ software. Values were obtained from z-stack projections (sum slices) and correspond to the median values of the pixels in the images after background subtraction. 3D views were performed with Imaris software (Bitplane).

RNA sequencing

RNAseq experiments were performed by Acobiom (Grabels, France). RNA extraction was performed using miRNeasy kit (Qiagen, Courtaboeuf, France), with on-column DNase digestion according to manufacturer's instructions. Briefly, educated spheroids were homogenized in 700 µl QIAzol® Lysis Reagent in a 2-ml SafeLock microcentrifuge tube. One 2-mm stainless steel bead was added to each sample and they were disrupted by mechanically using TissueLyzer (Qiagen) 2 × 2 min at 20 Hz. Samples were then incubated 5 min at room temperature. One hundred forty microliters chloroform was added to the homogenate. Tubes were shaked vigorously for 15 s, and they were placed back onto the benchtop for another 3 min. Lysates were centrifuged at 12,000 x *g* for 15 min at 4 °C in a microcentrifuge. Upper aqueous phases were carefully transferred to clean 2-ml microcentrifuge tubes. RNA was eluted in water and immediately stored at − 80 °C until use. The full procedure was performed using QIAcube automated workstation (QIAcube–QIAGEN) to optimize reproducibility of RNA extraction. RNA integrity was assessed using Agilent 2200 TapeStation with

RNA ScreenTapes. RINe (RNA Integrity Number equivalent) scores were > 7.7 for all samples. RNA-seq libraries were prepared following the protocol TruSeq Stranded Total RNA and validated on labchip GX platform. Human GRCh38.p13 genome was used as a reference. RNA-Seq data were mapped and annotated using Ensembl database release 108 (https://www.ensembl.org).

Graphs and statistics

Plots and statistics were generated using GraphPad Prism v9 (Dotmatics, San Diego, CA); otherwise, Excel (Microsoft Office 364).

Results

We used depleted serum prepared from blood sampling of healthy donors to educate spheroids containing human hepatic and human stellate cell lines (HepG2 and TWNT-1) (Fig. 1A). By adding depleted human serum to the cell culture medium, we observed that the rate of autonomous spheroid formation varies between donors, and their shapes are different after 3 days of culture (Fig. 1B). Confocal microscopy analysis revealed that the spheroids are positive for ZO-1, a tight junction protein [14], and MRP2, an ATP-binding cassette transporter that has an important role in the detoxification and chemoprotection [15], suggesting that educated spheroids contain functional bile canalicular structures (Fig. 1C). We showed also that the level of activation of hepatic stellate cells is donor-dependent (Fig. 1D), and consequently, we observed that the amount of spontaneous deposition of extracellular matrix (ECM), such as type I collagen and fibronectin, varies also between donors (Fig. 1E).

To further characterize donor-dependent educated spheroids, their molecular signatures were assessed by RNAseq. Principal component analysis (PCA) showed a clear separation of educated spheroids from non-educated spheroids (Fig. 2A). Analysis of differentially expressed genes (DEGs) indicates that the expression of 1460 genes differs between educated and non-educated spheroids. Among those 1460 DEGs, we found that 591 genes (40.5%) were upregulated while 869 DEGs (59.5%) were downregulated after the educating step (Fig. 2B). Gene Ontology analysis showed that these differentially expressed genes are assigned to biological regulation, cellular, metabolic, signaling, ATP-dependent, response to stimuli, and binding processes, as well as to catalytic, regulatory, and transport activities (Fig. 2C). Interestingly, we found also that educated spheroids showed

an increase in CYP3A4 basal activity by 2 to 19 times as compared to non-educated spheroids (Fig. 2D).

The induction of the activity of CYP3A4 that metabolizes about half of all drugs on the market [16] was assessed after treatment for 4 days with bosentan and rifampicin. As expected, we found an enhanced metabolizing CYP activity in a donor-dependent manner, ranging from 1.5 to 80 times upon bosentan treatment (Fig. 3A) and from 1.5 to 55 times upon rifampicin treatment (Fig. 3B). Our data indicate that donor-dependent educated spheroids may be valuable experimental tools for predicting drug metabolism and thus drug-induced liver injury.

To test whether donor-dependent educated spheroids could estimate the actual DILI in a population, we experimentally generated treatment groups of 24 randomly selected individuals (from $n = 109$ donors) and performed a DILI risk prediction. The number of donors included in each group was determined based on the study published by Fermini and colleagues, where the authors reported that a sample size of 24 is sufficient to have 92% of chance to detect an event with 10% incidence [17]. The age, the sex, and the ABO blood type of the donors are reported in Table 1. Educated spheroids were treated with a panel of drugs with clinical apparent DILI. These drugs are known as difficult-to-detect DILI compounds by current preclinical models. The concentrations of the drugs used range from $0.01 \times C_{max}$ to $100 \times C_{max}$. DILI risk is determined using the numerical margin of safety (MOS) [18–21] calculated with the drug concentration that induced at least 20% of cell death. ROC curve analysis showed that MOS_{20} can discriminate DILI-positive drugs from DILI-negative drugs with an optimal cut point at $100 \times C_{max}$ and an area under the curve (AUC) of 0.8726 (Fig. 4A). For each drug and for each donor included in the study, we generated an inhibitory dose-response curve fit with constrains (top = 100; bottom = 0) and calculated the LogIC50 and HillSlope values (Table 2). The DILI risk is estimated by using the toxicity score (TS) that is calculated with the formula reported in Table 2. A drug is considered as at clinical DILI risk if at least 10% of individuals within the cohort are categorized as DILI positive (based on the TS) (Table 2). As expected, we found a variation in the susceptibility to drug-induced liver injury between donors. We observed that in the cohorts that were treated with albuterol or with flavoxate, only 8.3% and 4.2% of donors were DILI positive confirming that these drugs have no clinical DILI concerns (Fig. 4B). In contrast, in cohorts that were treated with etoposide, β-estradiol, nizatidine, azathioprine, oxaliplatin, bosentan, and stavudine, 75%, 54.2%, 54.2%, 91.7%, 100%, 100%, and 45.8% of donors,
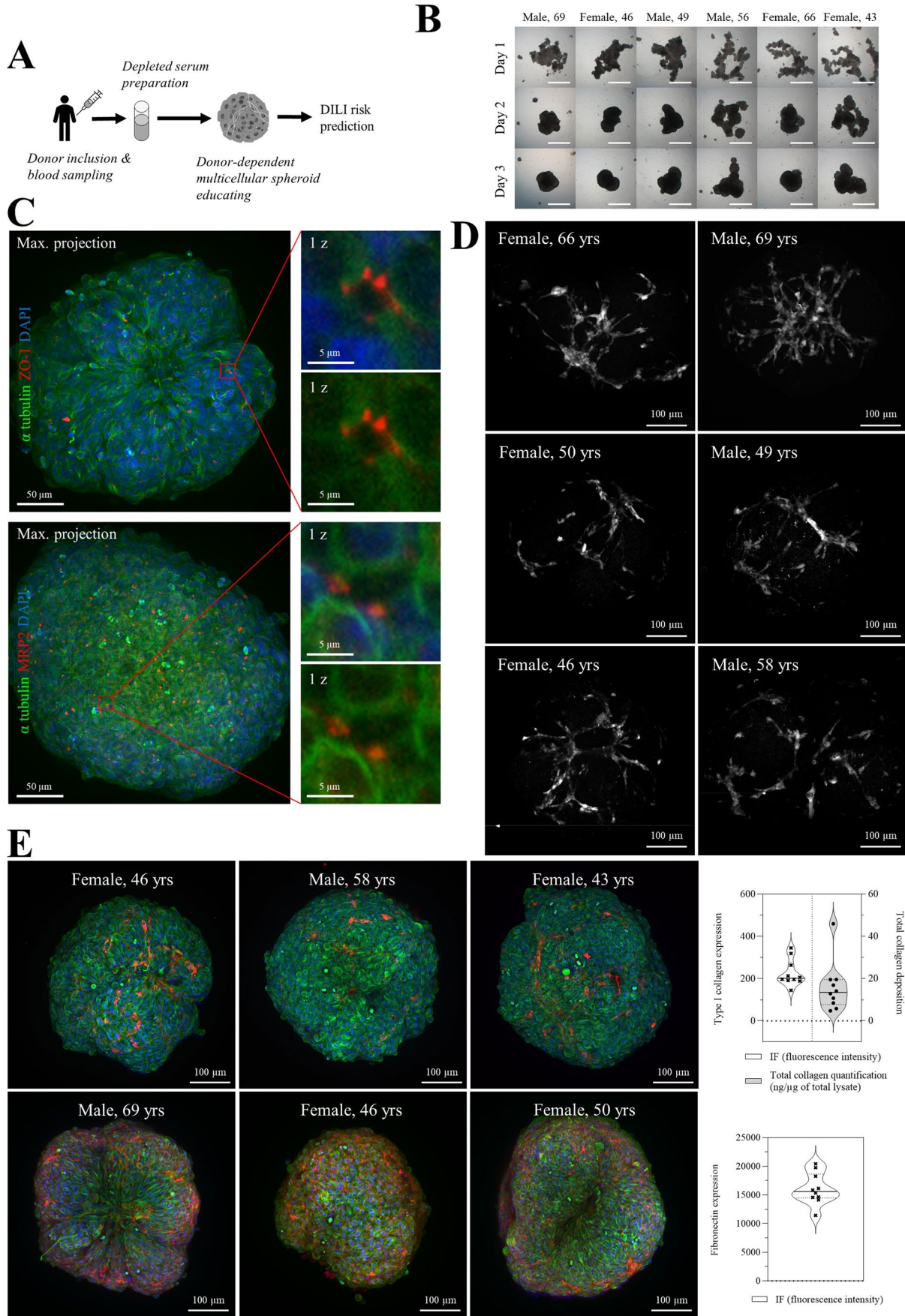
◀**Fig. 1** Donor-dependent educated spheroids display a distinct phenotype and ECM production. **A** Workflow of cell line-based spheroids educating. **B** Spheroids were educated for 3 days with donor's sera. Pictures show the phenotypes at days 1, 2, and 3. Scale bar: 250 μm. **C** Formation of bile canalicular structure. Educated spheroids were generated with the depleted serum of a 41-year-old female and then stained for ZO-1 and MRP2. **D** Activation of hepatic stellate cells. Educated spheroids from 6 different donors were stained for α-SMA after 3 days of culture. Scale bar: 100 μm. **E** Educated spheroids from different donors were stained for type 1 collagen, fibronectin, and α-tubulin after 3 days of culture. Violin plots (upper right) show a quantification of type 1 collagen protein deposition by immunofluorescence and by colorimetric assay for 10 different donors. Violin plot (lower right) shows the quantification of fibronectin deposition for 10 different donors. Each dot corresponds to one donor. Solid line is the median. Dotted thin black lines show quartiles

were DILI positive, respectively, confirming that these drugs are clinically at high risk for DILI development (Fig. 4B; Table 3).

Idiosyncratic DILI is generally difficult to predict and is usually not dose related contrary to intrinsic DILI that develops in a dose-dependent manner [22]. Interestingly, we found that azathioprine, a well-known iDILI drug [23], induces a reduction of about 35% of cell viability up to a concentration of $10\times C_{max}$. This decrease of cell viability then remained unchanged even at higher doses of azathioprine while sorafenib displayed a clear dose-dependent reduction of cell viability (Fig. 4C). Our data suggest that
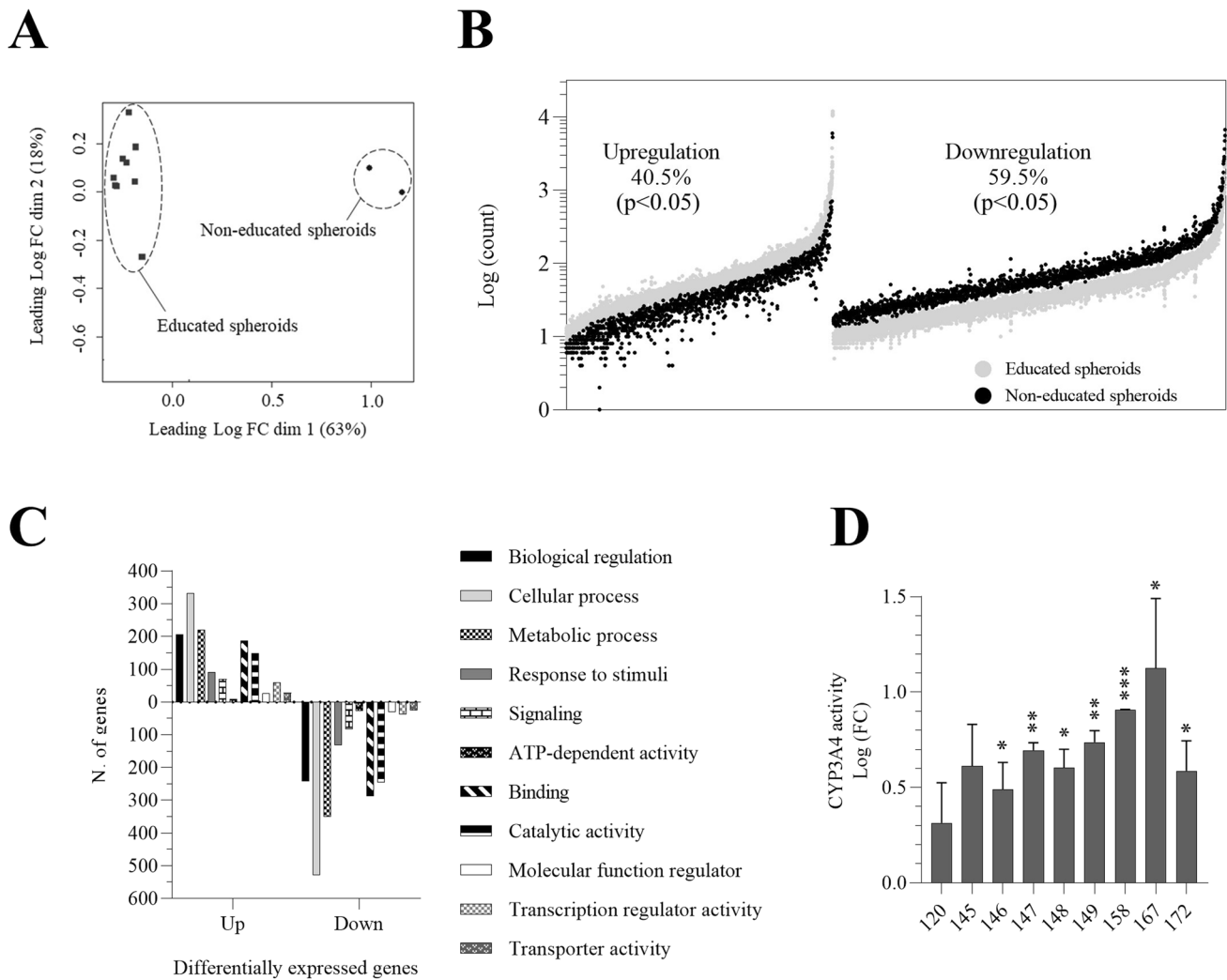
Fig. 2 Alteration of the transcriptomic profile and upregulation of the basal CYP3A4 activity in educated spheroids. **A** Principal component analysis separates transcripts from educated and non-educated spheroids. Educated spheroids from 10 different donors and non-educated spheroids were sequenced after 3 days of culture. **B** Analysis of differentially expressed genes (DEGs). 1460 DEGs were found after the educating step. Fisher's t-test **C** Gene Ontology (GO) analysis of DEGs using PANTHER classification system. Graph shows the number of differentially expressed genes compared to non-educated condition with $p < 0.05$. **D** Increased CYP3A4 basal activity in educated spheroids as compared to non-educated spheroids. CYP3A4 activity was measured after 3 days of culture. Shown are the results from 9 donors. Results are expressed as mean ± s.e.m. of Log fold change to non-educated spheroids. *$p < 0.05$, **$p < 0.01$, ***$p < 0.001$, Fisher's t-test

Fig. 3 Induction of drug metabolizing capacity in educated spheroids. CYP3A4 activity was measured in educated spheroids from 9 different donors after 4 days of exposure to bosentan (**A**) or to rifampicin (**B**). Results are shown as Log relative luminescence. Educated spheroids significantly increased CYP3A4 activity in response to bosentan and rifampicin. **$p < 0.01$, ***$p < 0.001$, Mann-Whitney t-test
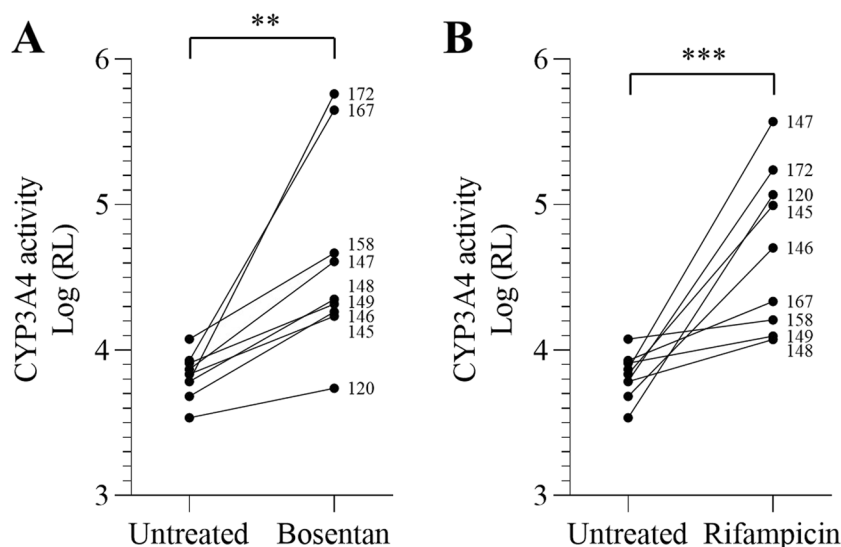
donor-dependent educated spheroids might be capable of predicting iDILI risk.

Next, we assessed the reliability of our educated spheroid system to predict DILI risk. For that, we performed 2 independent experiments including 10 donors in the first cohort and 23 donors in the second cohort. Educated spheroids were treated with sorafenib, and we calculated the TS for each donor. As expected, we found that all donors from both cohorts were DILI positive upon exposure to sorafenib demonstrating that our results are consistent between 2 independent experiments (Fig. 4D).

The performance of educated spheroids to predict DILI risk was assessed by comparing our results to those obtained from other in vitro and in vivo models. We found that educated spheroids correctly predicted clinical DILI in 9 drugs out of 9 and did not falsely mark albuterol, flavoxate, and lenvatinib as toxic, yielding a sensitivity and a specificity of 100% (Fig. 5). Meanwhile, other in vitro models and animal models were not capable to detect β-estradiol and stavudine-mediated DILI. Taken together, these data demonstrate that the educated spheroid system is more sensitive than current preclinical models to predict clinical DILI risk.

As non-genetic host factors that are associated to DILI development are age [24, 25] and sex [26–28], we analyzed age- and sex-associated DILI risk and DILI severity upon treatment with clinical DILI positive drugs. Figure 6 shows the risk for DILI development and the degree of severity (ranked accordingly to the TS) for each donor included in the study. As expected, cohorts treated with non-toxic drugs (flavoxate, albuterol, and lenvatinib) did not have more than 2 donors out of 24 (8.3%) who displayed a low DILI-positive risk while those treated with DILI-positive drugs have at least 11 donors (stavudine) out of 24 (45.8%) who

showed a clear DILI-positive risk at different degrees of severity (Fig. 6). We then analyzed how much age and sex influence DILI risk and severity. We found that DILI risk is associated with the sex of the donor for β-estradiol ($\eta_p^2 = 0.1595$, $p = 0.0532$), while it is associated with the age of the donor for nizatidine ($\eta_p^2 = 0.3414$, $p = 0.0027$) (Fig. 6; Table 4). From 9 DILI-positive drugs tested, we found that the severity of DILI is associated with the age of the donors for β-estradiol ($R^2 = 0.3298$, $p = 0.0401$) and oxaliplatin ($R^2 = 0.2247$, $p = 0.0193$) (Fig. 6, Table 4). Overall, our data confirm that age and sex are host risk factors for DILI for some medications [29–31].

Discussion

Drug-induced hepatotoxicity is a major challenge in drug development and personalized medicine [32]. Indeed, 90% of drugs that passed preclinical testing fail clinical trials because of liver toxicity [33]. Moreover, treatment discontinuation due to hepatotoxicity occurred in 20 to 40% of patients [34]. These observations suggest that an improvement of preclinical testing of DILI is urgently needed for the development of safer medications. We present here an easy to set up, to handle, and affordable model that reproduces the variability among people. This model makes possible the analysis of DILI risk in a population and thus de-risking failure when entering first-in-human trials. Furthermore, it also provides a way to give a more robust safety profile to a drug when it is used in an exploratory study in clinical trials phase 2.

One major drawback of currently available models to predict DILI risk is their inability to generate a functional

Table 1 Donor's characteristics

Donor #	Sex	Age	ABO blood type	Used in figure	Donor #	Sex	Age	ABO blood type	Used in figure
11	M	24	O	4D	89	M	25	O	4A, 4B, 4C, 5, 6
12	M	44	O	4D	90	M	27	O	4A, 4B, 4C, 5, 6
13	F	67	A	4D	91	F	24	O	4A, 4B, 4C, 5, 6
14	M	46	A	4D	92	M	51	B	4A, 4B, 4C, 5, 6
15	F	33	A	4D	93	F	23	O	4A, 4B, 4C, 5, 6
16	M	57	O	4D	94	F	38	O	4A, 4B, 4C, 5, 6
17	M	38	O	4D	95	M	59	O	4A, 4B, 4C, 5, 6
18	F	52	O	4D	96	M	42	O	4A, 4B, 4C, 5, 6
19	M	61	B	4D, 6	97	F	54	O	4A, 4B, 4C, 5, 6
20	M	52	A	4D	98	M	37	A	4A, 4B, 4C, 5, 6
21	M	69	B	1B, 1D, 2	99	F	27	O	4A, 4B, 4C, 5, 6
22	F	47	O	4A, 4B, 5, 6	100	F	23	O	4A, 4B, 4C, 5, 6
23	F	46	A	1B, 1D, 1E, 2	101	M	62	A	4A, 4B, 4C, 5, 6
24	F	43	A	1E, 2	102	F	30	O	4A, 4B, 4C, 5, 6
25	M	49	O	1B, 1D, 2	103	F	50	O	4A, 4B, 5, 6
26	M	56	A	1B, 1E, 2	104	M	26	B	4A, 4B, 5, 6
27	F	65	O	4A, 4B, 5, 6	105	F	41	A	4A, 4B, 5, 6
28	M	63	AB	4A, 4B, 5, 6	106	F	20	O	4A, 4B, 5, 6
29	F	50	A	4A, 4B, 5, 6	107	M	20	B	4A, 4B, 5, 6
30	F	66	O	1B, 1D, 1E, 2	108	F	30	A	4A, 4B, 5, 6
31	F	50	O	1D, 2	109	M	24	A	4A, 4B, 5, 6
32	F	55	A	4A, 4B, 5, 6	110	F	36	O	4A, 4B, 5, 6
33	F	43	B	1B, 1E, 2	111	F	50	A	4A, 4B, 5, 6
34	M	58	A	1D, 1E, 2	112	M	63	O	4A, 4B, 5, 6
35	F	41	O	4A, 4B, 5, 6	113	F	22	B	4A, 4B, 5, 6
36	F	51	A	4A, 4B, 5, 6	114	M	18	B	4A, 4B, 5, 6
37	M	51	A	4A, 4B, 5, 6	115	M	30	O	4A, 4B, 5, 6
38	F	36	O	1E, 4A, 4B, 5, 6	118	F	21	A	6
39	F	36	A	4A, 4B, 5, 6	119	F	23	O	6
39	F	36	A	6	120	F	20	A	2D, 3A, 3B, 6
40	M	50	O	4A, 4B, 5, 6	121	F	45	A	4A, 4B, 5, 6
41	F	38	O	4A, 4B, 5, 6	122	F	65	A	4A, 4B, 5, 6
42	M	50	A	4A, 4B, 5, 6	123	F	50	O	4A, 4B, 5, 6
43	F	70	A	4A, 4B, 5, 6	124	F	64	A	4A, 4B, 5, 6
44	F	34	A	4A, 4B, 5, 6	125	M	60	AB	4A, 4B, 5, 6
45	M	38	A	4A, 4B, 5, 6	126	F	49	AB	4A, 4B, 5, 6
46	F	46	A	4A, 4B, 5, 6	127	M	63	AB	4A, 4B, 5, 6
47	F	46	O	4A, 4B, 5, 6	128	M	58	AB	4A, 4B, 5, 6
48	F	34	O	4A, 4B, 5, 6	129	F	40	O	4A, 4B, 5, 6
49	F	60	A	4A, 4B, 5, 6	130	F	36	O	4A, 4B, 5, 6
50	F	32	O	4A, 4B, 5, 6	131	F	44	AB	4A, 4B, 5, 6
51	F	33	A	4A, 4B, 5, 6	132	M	47	AB	4A, 4B, 5, 6
52	F	56	A	4A, 4B, 5, 6	133	F	57	O	4A, 4B, 5, 6
53	M	32	O	4A, 4B, 5, 6	134	M	62	AB	4A, 4B, 5, 6
54	F	30	O	4A, 4B, 5, 6	135	F	41	AB	1C
55	M	55	A	4A, 4B, 5, 6	135	F	41	AB	4A, 4B, 5, 6
56	F	48	O	4A, 4B, 5, 6	136	M	52	AB	4A, 4B, 5, 6
57	F	44	A	4A, 4B, 5, 6	137	M	46	AB	4A, 4B, 5, 6
58	M	42	B	2	138	F	36	AB	4A, 4B, 5, 6

Table 1 (continued)

Donor #	Sex	Age	ABO blood type	Used in figure	Donor #	Sex	Age	ABO blood type	Used in figure
59	F	43	A	4A, 4B, 5, 6	139	F	35	AB	4A, 4B, 5, 6
60	F	28	O	4A, 4B, 5, 6	140	M	58	AB	4A, 4B, 5, 6
61	F	29	A	4A, 4B, 5, 6	141	M	39	AB	4A, 4B, 5, 6
62	F	38	O	4A, 4B, 5, 6	142	M	46	AB	4A, 4B, 5, 6
63	F	49	O	4A, 4B, 5, 6	143	F	36	O	4A, 4B, 5, 6
64	F	29	O	4A, 4B, 5, 6	144	M	50	AB	4A, 4B, 5, 6
65	M	45	A	4A, 4B, 5, 6	144	M	50	AB	4A, 4B, 5, 6
66	F	43	A	4A, 4B, 5, 6	145	M	52	A	2D, 3A, 3B, 4C, 4D, 6
67	F	43	B	4A, 4B, 5, 6	146	M	30	AB	2D, 3A, 3B, 4C, 4D, 6
68	F	31	A	4A, 4B, 5, 6	147	M	48	A	2D, 3A, 3B, 4C, 4D, 6
69	F	28	A	4A, 4B, 5, 6	148	M	29	AB	2D, 3A, 3B, 4C, 4D, 6
70	M	27	O	4A, 4B, 5, 6	149	F	30	O	2D, 3A, 3B, 4C, 4D, 6
71	F	28	O	4A, 4B, 5, 6	150	F	33	AB	4C, 4D, 6
72	M	36	O	4A, 4B, 5, 6	151	M	28	O	4C, 4D, 6
73	F	26	O	4A, 4B, 5, 6	152	M	41	AB	4C, 4D, 6
74	F	24	A	4A, 4B, 5, 6	153	M	26	AB	4C, 4D, 6
75	F	57	O	4A, 4B, 5, 6	154	M	27	AB	4C, 4D, 6
76	M	30	O	4A, 4B, 5, 6	155	M	27	AB	4C, 4D, 6
77	M	20	O	4A, 4B, 5, 6	156	F	38	A	4C, 4D, 6
78	M	23	A	4A, 4B, 5, 6	157	F	45	AB	4C, 4D, 6
79	F	23	A	4A, 4B, 4C, 5, 6	158	F	65	O	2D, 3A, 3B, 4C, 4D, 6
80	F	55	O	4A, 4B, 4C, 5, 6	159	F	36	AB	4C, 4D, 6
81	M	31	A	4A, 4B, 4C, 5, 6	160	F	49	A	4C, 4D, 6
82	M	20	A	4A, 4B, 4C, 5, 6	161	F	43	A	4C, 4D, 6
83	F	26	O	4A, 4B, 4C, 5, 6	163	M	41	O	4C, 4D, 6
84	M	29	O	4A, 4B, 4C, 5, 6	164	M	37	AB	4C, 4D, 6
85	F	22	A	4A, 4B, 4C, 5, 6	165	F	25	O	4C, 4D, 6
86	M	26	A	4A, 4B, 4C, 5, 6	166	F	27	O	4C, 4D, 6
87	M	39	O	4A, 4B, 4C, 5, 6	167	M	47	O	2D, 3A, 3B, 4C, 4D, 6
88	M	52	A	4A, 4B, 4C, 5, 6	168	M	61	AB	4C, 4D, 6
					172	M	18	AB	2D, 3A, 3B

donor-dependent liver specific microenvironment. Indeed, cholestasis is the main cause of DILI and is associated with an alteration of bile canaliculi functions [35]. As such, these canalicular structures are required for cholestasis toxicity detection [36]. We showed that educated spheroids trigger a spontaneous formation of bile canaliculi suggesting that our model is able to predict cholestasis toxicity (Fig. 1). Moreover, we demonstrated that the magnitude and the pattern of hepatic stellate cells activation is donor-dependent, and consequently, we observed a spontaneous donor-dependent deposition of ECM components (collagen and fibronectin) that are well known to influence DILI

occurrence [37] (Fig. 1). In-depth analysis of the model revealed that important metabolic and signaling pathways were altered in educated spheroids (Fig. 2), including glycolysis and response to stimuli. Interestingly, we found a downregulation of genes that are associated with cancer in educated HepG2-based spheroids suggesting a trend towards normal primary human hepatocytes [38]. Finally, cell lines such as HepG2 or Huh7 are generally of limited use for predicting drug-induced hepatotoxicity because of the low expression of ADME genes as compared to the liver, making that they cannot detect drug toxicity mediated by metabolism [39]. We demonstrated that educating
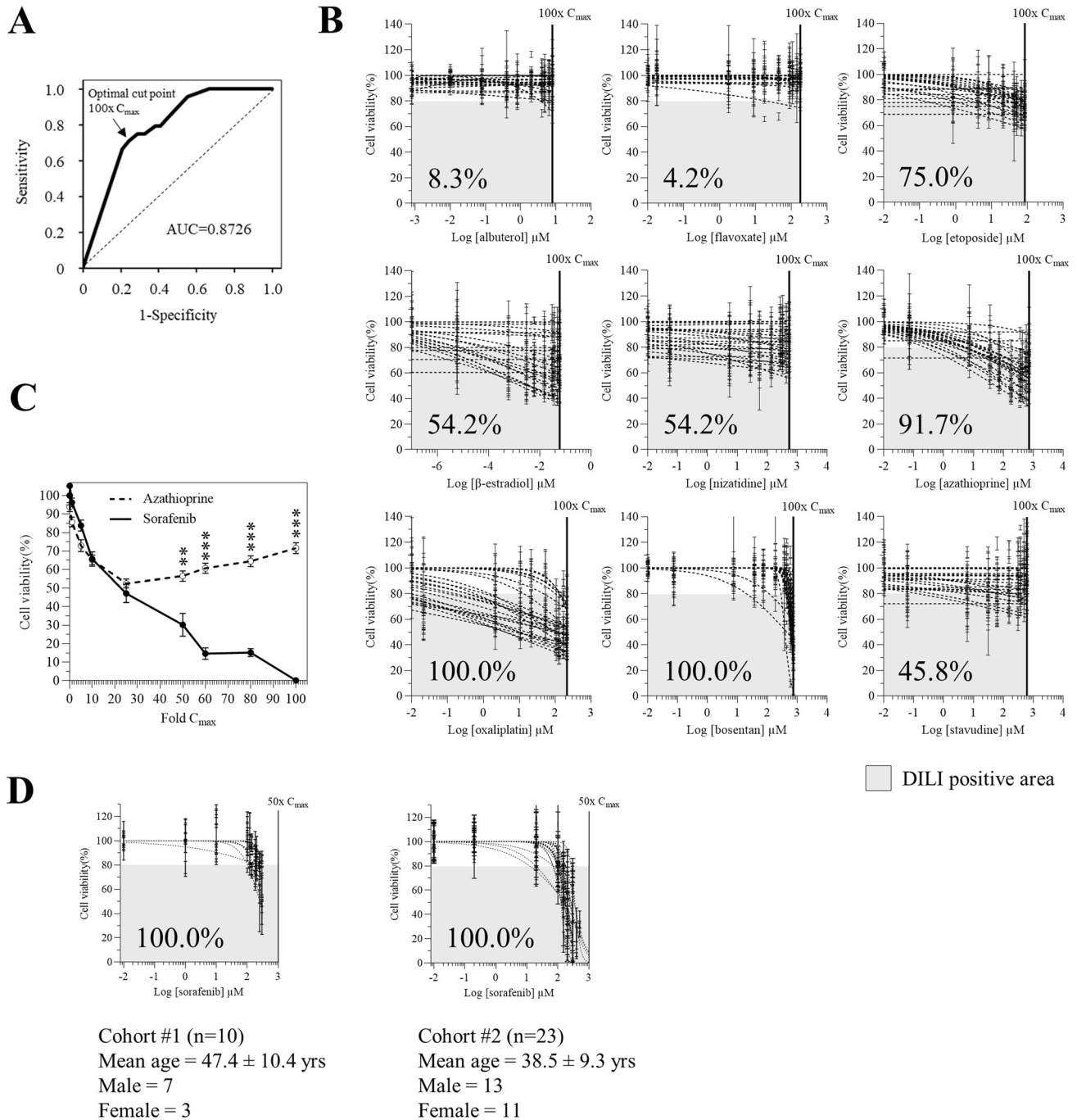
Fig. 4 Prediction of DILI risk by educated spheroids. **A** Receiver-operating curve (ROC) analysis of MOS_{20} as predictor of clinical DILI. ROC curve was generated from MOS_{20} of each donor of the independent groups, and the optimal cut point was determined. **B** Inhibitory dose-response curve fit with constrains (top = 100; bottom = 0) for each drug. DILI positive area is determined by the range [20% reduction of cell viability–$100 \times C_{max}$]. The percentage on the graph indicates the proportion of donors within a cohort of 24 donors, showing a DILI positive mark. Results are shown as percentage of cell viability of at least a triplicate. **C** Ability of educated spheroids to detect iDILI drug in dose-independent manner. For each drug, educated spheroids from 24 donors were used. Treatment duration was 96 h, and the concentrations range from $0.01 \times$ to $100 \times C_{max}$. Results are shown as percentage of cell viability of at least a triplicate. **$p <$ 0.01, ***$p <$ 0.001, Mann-Whitney t-test. **D** Reliability of educated spheroids to predict DILI risk. The experiment was performed on 2 independent cohorts. The concentrations used range from $0.01 \times$ to $50 \times C_{max}$

Table 2 Toxicity score (TS)

$$TS = LogIC_{50} - \frac{Log(0.25)}{HillSlope}$$

Cabozantinib — Non-linear curve fit with constrains (top=100 ; bottom=0), Cmax=10µM

Donor #	LogIC50	HillSlope	Toxicity Score (TS)
145	2.366	-1.824	2.03592325036844
146	2.368	-1.585	1.98815142502968
147	2.546	-4.863	2.422195765715
148	2.523	-2.205	2.24995692003267
149	2.176	-2.201	1.90246070362201
150	2.255	-1.824	1.92492325036844
151	2.022	-1.013	1.4276663461718
152	2.094	-4.537	1.96129997987041
153	2.276	-2.308	2.01514211814213
154	2.241	-2.605	2.00988292079541
155	2.346	-3.888	2.19114917918519
156	2.308	-3.564	2.13907183183839
157	2.302	-3.123	2.10921742192508
158	2.393	-2.14	2.11166355545422
159	2.38	-2.181	2.1039523194278
160	2.362	-2.386	2.10966974378543
161	2.1	-1.226	1.60892333496904
163	2.229	-2.515	1.98961232949186
164	2.292	-2.129	2.00920996179992
165	2.307	-4.592	2.17588937471081
166	2.219	-4.623	2.08876855043739
167	2.136	-8.27	2.06319951737268
168	2.546	-2.298	2.28400696634989

-5 < TS < Log(100 x Cmax) = DILI positive

Bosentan — Non-linear curve fit with constrains (top=100 ; bottom=0), Cmax=7.43µM

Donor #	LogIC50	HillSlope	Toxicity Score (TS)
121	2.803	-4.861	2.67914482795146
122	2.798	-8.076	2.72345071925112
123	2.785	-3.741	2.62406442359584
124	2.843	-4.056	2.69456311850888
125	2.845	-7.34	2.76297547802071
126	2.898	-2.94	2.6932176900245
127	2.783	-5.645	2.67634632571692
128	2.586	-4.543	2.45347523853666
129	2.769	-4.151	2.62396025263118
130	2.824	-6.048	2.72445304376191
131	2.867	-4.489	2.74721837088489
132	2.849	-11.02	2.79436660695754
133	2.877	-55.33	2.86611874224963
134	2.873	-59.2	2.86283006771406
135	2.834	-5.457	2.72367198253107
136	2.832	-3.345	2.65201196073902
137	2.991	-3.646	2.82587109398575
138	2.866	-5.488	2.75629519108456
139	2.877	-9.859	2.81593295554032
140	2.651	-0.4468	1.30350673382282
141	3.147	-0.2815	2.05926740500082
142	2.885	-12.94	2.83847295275673
143	2.788	-4.237	2.64590417953081
144	2.802	-3.584	2.63401451134822

-3 < TS < Log(100 x Cmax) = DILI positive

β-estradiol — Non-linear curve fit with constrains (top=100 ; bottom=0), Cmax=0.0006µM

Donor #	LogIC50	HillSlope	Toxicity Score (TS)
22	-0.5271	-1.746	-0.871922446350494
27	-1.48	-0.1533	-5.40733197213283
28	-2.34	-0.1253	-5.9194291993339
29	-2.386	-0.1253	-7.190948055291
32	-1609581	0.0000001133	3704275.94022915
35	-1922018	0.000000541	-809152.951334635
36	-2.667	-0.1745	-6.11720052336041
37	0.5915	-0.134	-3.90148500991017
38	-1194228	0.0000002945	850118.320298684
39	-2696903	0.00000008293	4562954.60675223
40	-0.7257	-0.1399	-5.02920243079959
41	1.535	-0.1252	-3.2737858732654
42	-1.745	-0.1867	-4.96974553469717
43	-2.391	-0.1769	-5.79439169772732
44	0.5447	-0.1095	-4.95356476098596
45	3.294	-0.06555	-5.8907443375738
46	-1099901	0.0000005472	354.832105194451
47	6.033	-0.1177	0.917791917349513
48	1.426	-0.1415	-2.8288409281281
49	21.32	-0.03882	5.81098425224208
50	5.127	-0.1673	1.5283150548389
51	3.671	-0.09386	-3.34344695640275
52	-0.2799	-0.1579	-4.09281951442661
53	-2224558	0.0000007884	-1460910.11652973

-7 < TS < Log(100 x Cmax) = DILI positive

Oxaliplatin — Non-linear curve fit with constrains (top=100 ; bottom=0), Cmax=4.1µM

Donor #	LogIC50	HillSlope	Toxicity Score (TS)
22	2.546	-1.401	2.11626410326341
27	2.02	-0.1015	-3.91162553032475
28	0.417	-0.145	-3.73513787122733
29	0.7145	-0.1051	-5.0139490135867
32	2.266	-0.1783	-1.11066848753765
35	3.125	-0.4141	1.67109996479314
36	0.3535	-0.1697	-3.19429016692966
37	2.56	-0.1878	-0.64585724881691
38	2.663	-0.1549	-1.22376559927671
39	0.8087	-0.1682	-2.7707291993339
40	1.948	-0.1265	-2.81136752037915
41	1.988	-0.2943	-0.0577356144341228
42	1.04	-0.1353	-3.4098151613301
43	0.7988	-0.1426	-3.42321957452989
44	2.117	-0.1466	-1.98982122324667
45	2.115	-0.2086	-0.771193630537145
46	1.693	-0.2722	-0.518829505246004
47	2.936	-0.647	2.00545905513452
48	2.459	-0.449	1.11810915071723
49	2.854	-0.794	2.09573804618645
50	3.112	-0.6575	2.1963190484354
51	2.717	-0.2107	-0.140427581053452
52	2.962	-0.1374	-1.41980488593859
53	2.648	-1.184	2.13950338570273

-5 < TS < Log(100 x Cmax) = DILI positive

Azathioprine — Non-linear curve fit with constrains (top=100 ; bottom=0), Cmax=7.2µM

Donor #	LogIC50	HillSlope	Toxicity Score (TS)
79	3.398	-0.1829	0.106255924942797
80	3.928	-0.2055	0.998267682102373
81	4.166	-0.2952	2.12650138439037
82	5.113	-0.4298	3.712208954565
83	3.465	-0.1471	-0.627861939687032
84	2.944	-0.2489	0.525116949264916
85	3.515	-0.2735	1.31448833578961
86	2.518	-0.2656	0.251207863976045
87	5.321	-0.1835	2.04001912082854
88	2.113	-0.2451	-0.343385113537178
89	1.618	-0.2125	-1.21522348660218
90	2.479	-0.1799	-0.867636972362214
91	1.999	-0.2264	-0.660275580070505
92	3.375	-0.2563	1.02595944487724
93	3.268	-0.4521	1.93630349186471
94	4.238	-0.1851	0.985379841556119
95	3.252	-0.2627	0.960184273589789
96	4.806	-0.2452	2.35061667484518
97	5.88	-0.2436	3.40848936236469
98	3.936	-0.168	0.352309575428795
99	3.186	-0.2815	1.04724337006052
100	3.05	-0.248	0.622338744645313
101	3.383	-0.2119	0.541754170231419
102	3.42	-0.2003	0.414208730264791

-5 < TS < Log(100 x Cmax) = DILI positive

Etoposide — Non-linear curve fit with constrains (top=100 ; bottom=0), Cmax=0.85µM

Donor #	LogIC50	HillSlope	Toxicity Score (TS)
79	2.82	-0.3406	1.05235469369359
80	3.16	-0.2161	0.373975051698462
81	2.934	-0.5493	1.83795049821962
82	-36.74	0.02941	-16.2687320187704
83	6.261	-0.126	1.48274610057173
84	7.671	-0.1225	2.75622456058806
85	3.732	-0.2436	1.26048936236469
86	3.589	-0.1617	-0.134314726827225
87	2.6	-0.6198	1.62862215016463
88	3.25	-0.1544	-0.649352275440171
89	2.941	-0.13	-1.69023070252279
90	3.961	-0.1294	-0.691704724327376
91	2.879	-0.128	-1.82459368224971
92	4.702	-0.1241	-0.149410083222904
93	6.258	-0.1532	2.32810449524829
94	4.928	-0.2034	1.96801970831877
95	6.92	-0.1185	1.83932496769652
96	-876868	0.000001353	-431886.48386699
97	-13.17	0.2223	-10.4616779517411
98	3.388	-0.3917	1.85095636628041
99	3.719	-0.3204	1.83991138786529
100	4.009	-0.1791	0.647414342110763
101	4.161	-0.2096	1.28857637725209
102	4.111	-0.2212	1.38920980412314

-5 < TS < Log(100 x Cmax) = DILI positive

Nizatidine — Non-linear curve fit with constrains (top=100 ; bottom=0), Cmax=5.43µM

Donor #	LogIC50	HillSlope	Toxicity Score (TS)
103	-1.139	-3.245	-1.32453466604868
104	9.787	-0.08074	2.33022527461033
105	-0.5132	-0.4291	-1.91627618580276
106	70.57	-3.124	70.3772791320973
107	-1481405	0.0000005319	-349500.522978074
108	3.553	-0.1194	-1.48937848683386
109	27.72	-0.04364	13.9239415369394
110	10.8	-0.09344	4.35672098321958
111	-1.128	-3.314	-1.30967169321906
112	-1.146	-3.317	-1.32750738357792
113	38.41	-0.02892	17.5911881310386
114	11.17	-0.07738	3.38943665898214
115	2.927	-7.253	2.84399159088267
121	2220	-0.09228	2213.47572614453
122	0.9916	-0.2363	-1.55626284946239
124	1.416	-0.2997	-0.592875513273148
125	7.484	-0.08949	0.756321026617919
126	-1.229	-3.419	-1.40509242214916
129	15.64	-0.0678	6.76005912495631
131	-299386	0.000003338	-119020.514281617
135	1829497	-0.000001092	1278160.01160443
138	10.55	-0.06213	0.859673405311205
139	1.317	-0.237	-1.22333751615174
144	6.646	-0.07373	-1.51973974403855

-5 < TS < Log(100 x Cmax) = DILI positive

Stavudine — Non-linear curve fit with constrains (top=100 ; bottom=0), Cmax=6.16µM

Donor #	LogIC50	HillSlope	Toxicity Score (TS)
103	7.947	-0.07966	0.389129157319076
104	11.11	-0.08959	4.38983043500433
105	-84.37	0.01653	-47.9477379716901
106	-10.91	0.4787	-9.65230208621692
107	6.941	-0.1046	1.18516834294491
108	-1.112	-3.25	-1.29724922810091
109	11.61	-0.0248	8.67025394859393
110	32.08	-0.03202	13.2773769104322
111	-1.107	-3.292	-1.28988578108383
112	20.91	-0.04674	8.02895611193919
113	5.622	-0.31	3.67087099571625
114	6.227	-0.1549	2.34023440072329
115	-801191	0.00002217	-523743.999388036
121	-7.2	2.855	-6.98912084366796
122	4.819	-0.09602	-1.451151961341
124	4.067	-0.401	0.327496948273526
125	2.314	-0.4005	0.810729110292229
126	17.37	-0.03855	1.752360795643
129	1810179	-0.000008281	1083141.21310474
131	-33.64	0.04192	-19.2778818862604
135	3.896	-1.235	3.40850203131339
138	39.97	-0.03158	20.9054024278669
139	4.445	-0.09336	-2.00358024987106
144	-1.154	-3.19	-1.34273353960124

-5 < TS < Log(100 x Cmax) = DILI positive

Sorafenib — Non-linear curve fit with constrains (top=100 ; bottom=0), Cmax=20µM

Donor #	LogIC50	HillSlope	Toxicity Score (TS)
145	2.366	-1.824	2.03592325036844
146	2.368	-1.585	1.98815142502968
147	2.546	-4.863	2.422195765715
148	2.523	-2.205	2.24995692003267
149	2.176	-2.201	1.90246070362201
150	2.255	-1.824	1.92492325036844
151	2.022	-1.013	1.4276663461718
152	2.094	-4.537	1.96129997987041
153	2.276	-2.308	2.01514211814213
154	2.241	-2.605	2.00988292079541
155	2.346	-3.888	2.19114917918519
156	2.308	-3.564	2.13907183183839
157	2.302	-3.123	2.10921742192508
158	2.393	-2.14	2.11166355545422
159	2.38	-2.181	2.1039523194278
160	2.362	-2.386	2.10966974378543
161	2.1	-1.226	1.60892333496904
163	2.229	-2.515	1.98961232949186
164	2.292	-2.129	2.00920996179992
165	2.307	-4.592	2.17588937471081
166	2.219	-4.623	2.08876855043739
167	2.136	-8.27	2.06319951737268
168	2.546	-2.298	2.28400696634989

-5 < TS < Log(100 x Cmax) = DILI positive

Albuterol — Non-linear curve fit with constrains (top=100 ; bottom=0), Cmax=0.08µM

Donor #	LogIC50	HillSlope	Toxicity Score (TS)
121	563858	-0.000003907	409760.228992075
122	152090	-0.000009821	90786.6712831725
123	-352416	0.0000044	-215584.183789099
124	-1858104	0.000001265	-1382167.24796209
125	-127249	0.00001528	-87847.1681068087
126	190287	-0.00000741	109037.338552232
127	-10.26	0.2356	-7.70456709962665
128	20.66	-0.05406	9.52311521775874
129	5.384	-0.1266	0.628391853649586
130	12.53	-0.0963	6.29297533069551
131	16.43	-0.06878	7.67658343518519
132	19.39	-0.05565	8.57131192582278
133	2.188	-1.491	1.78420389582296
134	22.91	-0.06195	13.1915174926883
135	-536104	0.00002265	-270293.849303328
136	26.13	-0.03662	9.68925747329431
137	-65.06	0.02239	-38.1703174931683
138	-146.8	0.008412	-75.2284365991486
139	2184	-0.09168	2177.4330280178
140	1.563	-0.6629	0.564393280265446
141	7.759	-0.09894	1.67389080557952
142	-9.167	0.3631	-7.50888931058121
143	6.488	-0.158	2.67749372577239
144	10.29	-0.1158	5.09086363274644

-5 < TS < Log(100 x Cmax) = DILI positive

Flavoxate — Non-linear curve fit with constrains (top=100 ; bottom=0), Cmax=1.79µM

Donor #	LogIC50	HillSlope	Toxicity Score (TS)
54	1380032	-0.000001806	1046665.4488771
55	26.86	-0.04716	14.0936727877871
56	59280	-0.00002654	36594.996558856
57	-175.4	1.549	-175.011323440072
59	3.841	-0.3823	3.03438157646307
60	12.6	-0.1228	7.6972313409775
61	-22640	0.009525	-22576.7916019603
62	2.405	-6.519	2.31264534570824
63	-15.01	0.1548	-11.1207257702328
64	-18.35	0.1403	-14.0587669898221
65	4.227	-0.891	3.55128732735358
66	7.064	-0.3095	5.11873346905343
67	4.151	-1.427	3.72909390937073
68	-730525	0.000001941	-420344.685048442
69	6.625	-0.3519	4.91411625084441
70	-156487	0.0000107	-100219.711090845
71	15.24	-0.07676	7.39659208796297
72	4.074	-0.8801	3.38991865546192
73	4.928	-0.4543	3.60275238536658
74	-10.5	0.3823	-8.92516350685859
75	6.029	-0.1248	1.20480135153876
76	309.1	-0.003609	142.278168099761
77	-14.84	0.1258	-10.0541495124963
78	-9.19	0.2641	-6.9103332399547

-5 < TS < Log(100 x Cmax) = DILI positive

Lenvatinib — Non-linear curve fit with constrains (top=100 ; bottom=0), Cmax=0.5µM

Donor #	LogIC50	HillSlope	Toxicity Score (TS)
37	-60.71	0.02031	-35.4239860845039
19	-131485	0.000006801	-42959.7843952415
38	-800274	0.000001316	-342781.605373889
32	-8.772	0.3403	-7.00279638163984
39	3113630	-0.000000762	2323525.02450399
35	549181	-0.000001509	150201.549153106
40	1613850	-0.000000116	1094832.76609658
36	Unstable	Unstable	
41	-559593	0.000001713	-208127.739446607
42	Unstable	Unstable	
118	-603.4	0.3125	-601.47340802775
43	Unstable	Unstable	
119	10.17	-0.1381	5.81040556605386
44	Unstable	Unstable	
120	-534095	0.000001835	-205996.912082854
45	-1576476	0.0000007785	-803116.987375771
123	Unstable	Unstable	
65	Unstable	Unstable	
140	Unstable	Unstable	1.61874481491764
154	2.237	-2.211	1.96469787818726
158	2.887	-0.7505	2.08478811537419
165	Unstable	Unstable	
167	3.625	-0.6538	2.70413736413588

-5 < TS < Log(100 x Cmax) = DILI positive
no TS = DILI negative

Table 3 DILI prediction

Drugs	Clinically apparent liver injury	Number of DILI positive within a cohort of 24 individuals (%)	Predicted DILI risk	C_{max} reference
Albuterol	No	8.3	No	Proctor et al. 2017 [20]. Arch Toxicol
Flavoxate	No	4.2	No	Proctor et al. 2017 [20]. Arch Toxicol
β-Estradiol	Yes	54.2	Yes	Bircsak et al. 2021 [43]. Toxicology
Etoposide	Yes	75.0	Yes	Sipes et al. 2017 [53]. Environ Sci Technol
Nizatidine	Yes	54.2	Yes	Sipes et al. 2017 [53]. Environ Sci Technol
Azathioprine	Yes	91.7	Yes	Proctor et al. 2017 [20]. Arch Toxicol
Oxaliplatin	Yes	100.0	Yes	Lurvink et al. 2021 [54]. Ann Surg Oncol
Bosentan	Yes	100.0	Yes	Proctor et al. 2017 [20]. Arch Toxicol
Stavudine	Yes	45.8	Yes	Proctor et al. 2017 [20]. Arch Toxicol
Lenvatinib	No	0.0	No	Ikeda et al. 2016 [55]. Clin Cancer Res
Cabozantinib	Yes	100.0	Yes	Jones et al. 2022 [56]. J Chromatogr Sci
Sorafenib	Yes	100.0	Yes	Brendel et al. 2011 [57]. Cancer Chemother Pharmacol

< 10% DILI-positive individuals in a cohort of 24 individuals = no DILI risk

spheroids with donor's depleted serum increased the basal CYP3A4 activity by 2 to 19 times (Fig. 2). Moreover, this activity was enhanced up to 80 times when educated spheroids were treated with a drug suggesting an upregulation of the drug metabolizing capacity of the cells (Fig. 3). This drug metabolizing capacity of educated spheroids was further confirmed by our results showing that educated spheroids can predict azathioprine- [40], nizatidine- [41], and etoposide- [42] mediated hepatoxicity, 3 compounds from which the mechanism of liver injury is primarily caused by

their toxic metabolites (Fig. 4). Taken together, our data demonstrate that educating spheroids with donor's depleted serum permits to obtain a functional donor-dependent liver specific microenvironment with an enhanced drug metabolizing capacity of HepG2 cells sufficiently to detect the hepatotoxicity induced by drug metabolites.

Primary human hepatocytes are generally used to study drug-induced liver injury. However, and despite they highly express AMDE genes, their capacity to predict DILI has shown limitations as they could not detect clinical DILI for
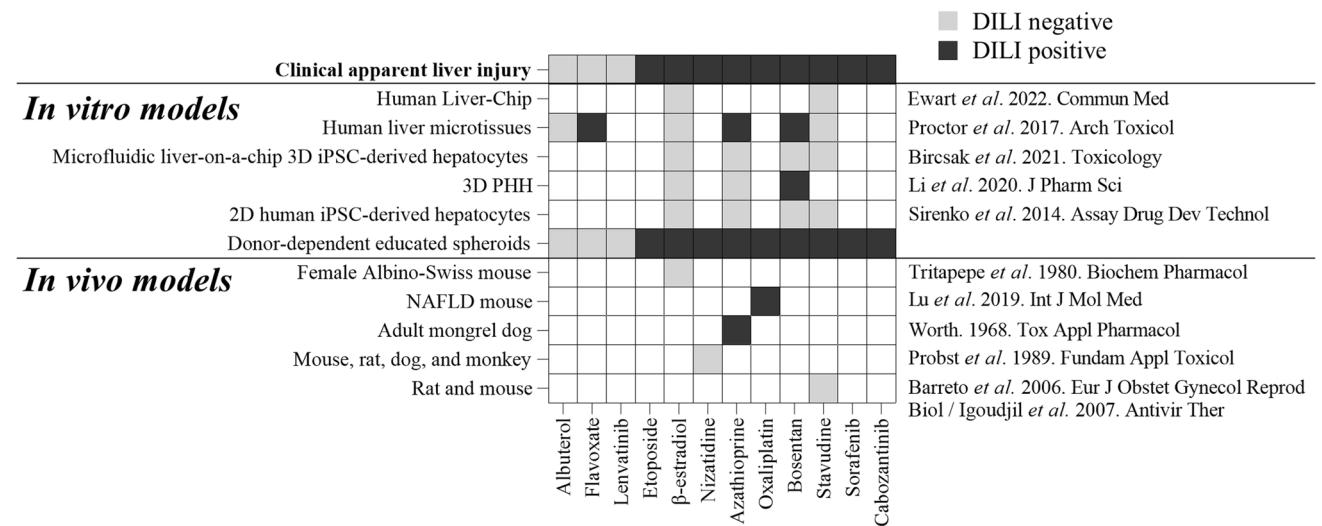
Fig. 5 High predictive power of clinical apparent DILI risk of educated spheroids. Comparative analysis to current in vitro and animal models. Educated spheroids were generated using depleted serum from 109 donors. For each treatment group, educated spheroids from 24 donors were used (Table 1). A panel of drugs with or without clinical DILI concerns was used to test drug-induced hepatotoxicity. Heatmap shows overall predicted DILI risk for each drug. To compare the performance between educated spheroids and current preclinical models in predicting DILI risk, we extracted the data from the works cited on the right side of the heatmap
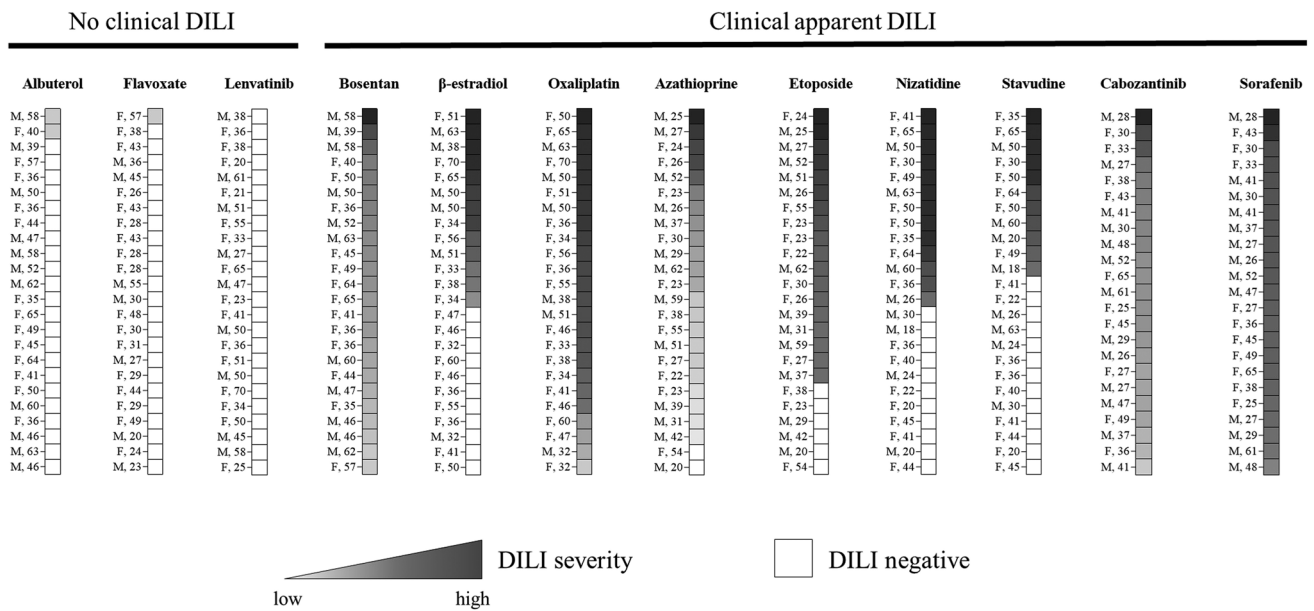
Fig. 6 DILI risk stratification and severity grades. Data from a panel of 12 drugs (3 without clinical apparent liver injury and 9 with clinical apparent hepatotoxicity) are reported as heatmaps. Each cell represents one donor. The sex and the age of the donor are reported on the left side of each cell. The degree of severity is determined by the TS (Table 2)

some drugs such as stavudine or β-estradiol [20]. Attempts to use liver organoids derived from pluripotent stem cells to assess DILI were also unsatisfactory, although they retain the genetic background of the donor from who they derived from [43–45]. Indeed, liver cancer organoids are difficult to generate and with a poor success rate, while healthy liver organoids are typically arranged as monolayer of cells forming cysts making them imperfect models [46, 47]. Moreover, liver organoids require artificially predefined amount of Matrigel or synthetic ECM scaffolds, and thus, they do not reproduce the donor-dependent composition of ECM [48]. All these constrains make that current in vitro models have a

limited capacity to predict DILI risk (Fig. 5). Animal models are also extensively used to analyze drug-induced hepatotoxicity. However, there are evidence that in vivo models are bad predictors of drug-induced toxicity in human [1] (Fig. 5). With a high sensitivity and specificity on the predictivity of clinical apparent DILI risk, educated spheroids appear to be a valuable option to analyze drug-induced liver injury easily and accurately, helping drug development pipelines.

Non-genetic factors contribute to the development of DILI too [49]. Indeed, elderly people are generally considered at high risk for DILI for some drugs [24], and an age cut-off point was estimated at 52 years old for high risk of adverse

Table 4 Sex- and age-associated DILI risk

	Bosentan	β-Estradiol	Oxaliplatin	Azathioprine	Etoposide	Nizatidine	Stavudine	Cabozantinib	Sorafenib
Sex-associated DILI risk ($\eta p2$)	-	0.1595* ($p = 0.0532$)	-	0.0004081 ($p = 0.9253$)	0.006442 ($p = 0.7093$)	0.1009 ($p = 0.1303$)	0.08606 ($p = 0.1641$)	-	-
Age-associated DILI risk ($\eta p2$)	-	0.05065 ($p = 0.2904$)	-	0.001707 ($p = 0.8480$)	0.001493 ($p = 0.8577$)	0.3414* ($p = 0.0027$)	0.09124 ($p = 0.1514$)	-	-
Sex-associated DILI severity ($\eta p2$)	0.08351 ($p = 0.1708$)	0.08956 ($p = 0.3206$)	0.02346 ($p = 0.4749$)	0.0002726 ($p = 0.9419$)	0.01233 ($p = 0.6609$)	0.1967 ($p = 0.1291$)	0.1824 ($p = 0.1901$)	0.003898 ($p = 0.7772$)	0.003037 ($p = 0.8028$)
Age-associated DILI severity (R^2)	0.00926 ($p = 0.6546$)	0.3298* ($p = 0.0401$)	0.2247* ($p = 0.0193$)	0.04116 ($p = 0.3652$)	0.01185 ($p = 0.7111$)	0.1075 ($p = 0.2741$)	0.07678 ($p = 0.4094$)	0.06530 ($p = 0.2392$)	0.06480 ($p = 0.2411$)

According to Cohen's guidelines $\eta p2 > 0.13$ means large effect
https://doi.org/10.4324/9780203771587

drug reactions [47]. Sex is considered as a non-genetic risk factor for DILI for some medications as well [49–52]. The good performance of educated spheroids in predicting DILI risk based on the age and the sex of the donor (Fig. 6) makes this model interesting to preclinically fine tune the safety profile of the people for whom the medication is dedicated.

Last but not least advantage of the educated spheroid model is its affordability as compared to current sophisticated in vitro models such as primary liver cells or organoids. Indeed, using educated spheroids to assess clinical DILI risk is barely more expensive than cell lines, and it is clearly financially much competitive than PHH or organoids.

Conclusion

In summary, we describe here the first donor-dependent multicellular spheroid model that utilizes our patented cell education technology to assess, with a high specificity and sensitivity, the interindividual DILI risk. To our knowledge, this is a unique preclinical model that offers a way to analyze DILI risk based on non-genetic factors such as age or/and sex confirming therefore the safety of a drug before entering clinical trials. Thus, this new preclinical model will be of great interest for pharmaceutical companies that invest billions of dollars in drug development, reducing the cost and de-risking failures.

Declarations

References

1. Atkins JT, George GC, Hess K, Marcelo-Lewis KL, Yuan Y, Borthakur G, Khozin S, LoRusso P, Hong DS. Pre-clinical animal models are poor predictors of human toxicities in phase 1 oncology clinical trials. Br J Cancer. 2020;123:1496–501. https://doi.org/10.1038/s41416-020-01033-x.

2. Fosse V, Oldoni E, Bietrix F, Budillon A, Daskalopoulos EP, Fratelli M, Gerlach B, Groenen PMA, Holter SM, Menon JML, et al. Recommendations for robust and reproducible preclinical research in personalised medicine. BMC Med. 2023;21:14. https://doi.org/10.1186/s12916-022-02719-0.

3. Chen L, Manautou JE, Rasmussen TP, Zhong XB. Development of precision medicine approaches based on inter-individual variability of BCRP/ABCG2. Acta Pharm Sin B. 2019;9:659–74. https://doi.org/10.1016/j.apsb.2019.01.007.

4. Ma Q, Lu AY. Pharmacogenetics, pharmacogenomics, and individualized medicine. Pharmacol Rev. 2011;63:437–59. https://doi.org/10.1124/pr.110.003533.

5. Silvestri A, Vicente F, Vicent MJ, Stechmann B, Fecke W. Academic collaborative models fostering the translation of physiological in vitro systems from basic research into drug discovery. Drug Discov Today. 2021;26:1369–81. https://doi.org/10.1016/j.drudis.2021.02.024.

6. Doyle LM, Wang MZ. Overview of extracellular vesicles, their origin, composition, purpose, and methods for exosome isolation and analysis. Cells. 2019;8 https://doi.org/10.3390/cells8070727.

7. Jung HH, Kim JY, Lim JE, Im YH. Cytokine profiling in serum-derived exosomes isolated by different methods. Sci Rep. 2020;10:14069. https://doi.org/10.1038/s41598-020-70584-z.

8. Martinez VG, O'Neill S, Salimu J, Breslin S, Clayton A, Crown J, O'Driscoll L. Resistance to HER2-targeted anti-cancer drugs is associated with immune evasion in cancer cells and their derived extracellular vesicles. Oncoimmunology. 2017;6:e1362530. https://doi.org/10.1080/2162402X.2017.1362530.

9. Pradere JP, Troeger JS, Dapito DH, Mencin AA, Schwabe RF. Toll-like receptor 4 and hepatic fibrogenesis. Semin Liver Dis. 2010;30:232–44. https://doi.org/10.1055/s-0030-1255353.

10. Ramadori G, Armbrust T. Cytokines in the liver. Eur J Gastroenterol Hepatol. 2001;13:777–84. https://doi.org/10.1097/00042737-200107000-00004.

11. Schwabe RF, Seki E, Brenner DA. Toll-like receptor signaling in the liver. Gastroenterology. 2006;130:1886–900. https://doi.org/10.1053/j.gastro.2006.01.038.

12. Soderberg A, Barral AM, Soderstrom M, Sander B, Rosen A. Redox-signaling transmitted in trans to neighboring cells by melanoma-derived TNF-containing exosomes. Free Radic Biol Med. 2007;43:90–9. https://doi.org/10.1016/j.freeradbiomed.2007.03.026.

13. Wang R, Tang R, Li B, Ma X, Schnabl B, Tilg H. Gut microbiome, liver immunology, and liver diseases. Cell Mol Immunol. 2021;18:4–17. https://doi.org/10.1038/s41423-020-00592-6.

14. Rao RK, Samak G. Bile duct epithelial tight junctions and barrier function. Tissue Barriers. 2013;1:e25718. https://doi.org/10.4161/tisb.25718.

15. Marin JJG, Monte MJ, Macias RIR, Romero MR, Herraez E, Asensio M, Ortiz-Rivero S, Cives-Losada C, Di Giacomo S, Gonzalez-Gallego J, et al. Expression of chemoresistance-associated ABC proteins in hepatobiliary, pancreatic and gastrointestinal cancers. Cancers (Basel). 2022;14 https://doi.org/10.3390/cancers14143524.

16. Zhou SF. Drugs behave as substrates, inhibitors and inducers of human cytochrome P450 3A4. Curr Drug Metab. 2008;9:310–22. https://doi.org/10.2174/138920008784220664.

17. Fermini B, Coyne ST, Coyne KP. Clinical trials in a dish: a perspective on the coming revolution in drug development. SLAS Discov. 2018;23:765–76. https://doi.org/10.1177/2472555218775028.

18. Albrecht W, Kappenberg F, Brecklinghaus T, Stoeber R, Marchan R, Zhang M, Ebbert K, Kirschner H, Grinberg M, Leist M, et al. Prediction of human drug-induced liver injury (DILI) in relation to oral doses and blood concentrations. Arch Toxicol. 2019;93:1609–37. https://doi.org/10.1007/s00204-019-02492-9.

19. Chen M, Borlak J, Tong W. High lipophilicity and high daily dose of oral medications are associated with significant risk for drug-induced liver injury. Hepatology. 2013;58:388–96. https://doi.org/10.1002/hep.26208.

20. Proctor WR, Foster AJ, Vogt J, Summers C, Middleton B, Pilling MA, Shienson D, Kijanska M, Strobel S, Kelm JM, et al. Utility of spherical human liver microtissues for prediction of clinical drug-induced liver injury. Arch Toxicol. 2017;91:2849–63. https://doi.org/10.1007/s00204-017-2002-1.

21. Shah F, Leung L, Barton HA, Will Y, Rodrigues AD, Greene N, Aleo MD. Setting clinical exposure levels of concern for drug-induced liver injury (DILI) using mechanistic in vitro assays. Toxicol Sci. 2015;147:500–14. https://doi.org/10.1093/toxsci/kfv152.

22. Roth RA, Ganey PE. Intrinsic versus idiosyncratic drug-induced hepatotoxicity--two villains or one? J Pharmacol Exp Ther. 2010;332:692–7. https://doi.org/10.1124/jpet.109.162651.

23. LiverTox: clinical and research information on drug-induced liver injury, Bethesda (MD). 2012.

24. Lucena MI, Sanabria J, Garcia-Cortes M, Stephens C, Andrade RJ. Drug-induced liver injury in older people. Lancet Gastroenterol Hepatol. 2020;5:862–74. https://doi.org/10.1016/S2468-1253(20)30006-6.

25. Mitchell SJ, Hilmer SN. Drug-induced liver injury in older adults. Ther Adv Drug Saf. 2010;1:65–77. https://doi.org/10.1177/2042098610386281.

26. Amacher DE. Female gender as a susceptibility factor for drug-induced liver injury. Hum Exp Toxicol. 2014;33:928–39. https://doi.org/10.1177/0960327113512860.

27. Floreani A, Bizzaro D, Shalaby S, Taliani G, Burra P, Special Interest Group Gender in Hepatology of the Italian Association for the Study of the L. Sex disparity and drug-induced liver injury. Dig Liver Dis; 2022. https://doi.org/10.1016/j.dld.2022.06.025.

28. Katarey D, Verma S. Drug-induced liver injury. Clin Med (Lond). 2016;16:s104–9. https://doi.org/10.7861/clinmedicine.16-6-s104.

29. Lucena MI, Andrade RJ, Kaplowitz N, Garcia-Cortes M, Fernandez MC, Romero-Gomez M, Bruguera M, Hallal H, Robles-Diaz M, Rodriguez-Gonzalez JF, et al. Phenotypic characterization of idiosyncratic drug-induced liver injury: the influence of age and sex. Hepatology. 2009;49:2001–9. https://doi.org/10.1002/hep.22895.

30. Mennecozzi M, Landesmann B, Palosaari T, Harris G, Whelan M. Sex differences in liver toxicity-do female and male human primary hepatocytes react differently to toxicants in vitro? PLoS One. 2015;10:e0122786. https://doi.org/10.1371/journal.pone.0122786.

31. Sgro C, Clinard F, Ouazir K, Chanay H, Allard C, Guilleminet C, Lenoir C, Lemoine A, Hillon P. Incidence of drug-induced hepatic injuries: a French population-based study. Hepatology. 2002;36:451–5. https://doi.org/10.1053/jhep.2002.34857.

32. Babai S, Auclert L, Le-Louet H. Safety data and withdrawal of hepatotoxic drugs. Therapie. 2021;76:715–23. https://doi.org/10.1016/j.therap.2018.02.004.

33. Sun D, Gao W, Hu H, Zhou S. Why 90% of clinical drug development fails and how to improve it? Acta Pharm Sin B. 2022;12:3049–62. https://doi.org/10.1016/j.apsb.2022.02.002.

34. Suzuki A, Andrade RJ, Bjornsson E, Lucena MI, Lee WM, Yuen NA, Hunt CM, Freston JW. Drugs associated with hepatotoxicity and their reporting frequency of liver adverse events in VigiBase: unified list based on international collaborative work. Drug Saf. 2010;33:503–22. https://doi.org/10.2165/11535340-000000000-00000.

35. Kawamoto T, Ito Y, Morita O, Honda H. Mechanism-based risk assessment strategy for drug-induced cholestasis using the transcriptional benchmark dose derived by toxicogenomics. J Toxicol Sci. 2017;42:427–36. https://doi.org/10.2131/jts.42.427.

36. Horiuchi S, Kuroda Y, Oyafuso R, Komizu Y, Takaki T, Maeda K, Ishida S. Construction of a culture protocol for functional bile canaliculi formation to apply human iPS cell-derived hepatocytes for cholestasis evaluation. Sci Rep. 2022;12:15192. https://doi.org/10.1038/s41598-022-19469-x.

37. Sasikumar S, Chameettachal S, Kingshott P, Cromer B, Pati F. Influence of liver extracellular matrix in predicting drug-induced liver injury: an alternate paradigm. ACS Biomater Sci Eng. 2022;8:834–46. https://doi.org/10.1021/acsbiomaterials.1c00994.

38. Tyakht AV, Ilina EN, Alexeev DG, Ischenko DS, Gorbachev AY, Semashko TA, Larin AK, Selezneva OV, Kostryukova ES, Karalkin PA, et al. RNA-Seq gene expression profiling of HepG2 cells: the influence of experimental factors and comparison with liver tissue. BMC Genomics. 2014;15:1108. https://doi.org/10.1186/1471-2164-15-1108.

39. Berger B, Donzelli M, Maseneni S, Boess F, Roth A, Krahenbuhl S, Haschke M. Comparison of liver cell models using the basel phenotyping cocktail. Front Pharmacol. 2016;7:443. https://doi.org/10.3389/fphar.2016.00443.

40. Lennard L, Van Loon JA, Weinshilboum RM. Pharmacogenetics of acute azathioprine toxicity: relationship to thiopurine methyltransferase genetic polymorphism. Clin Pharmacol Ther. 1989;46:149–54. https://doi.org/10.1038/clpt.1989.119.

41. NizatidineLiverTox: clinical and research information on drug-induced liver injury, Bethesda (MD). 2012.

42. EtoposideLiverTox: clinical and research information on drug-induced liver injury, Bethesda (MD). 2012.

43. Bircsak KM, DeBiasio R, Miedel M, Alsebahi A, Reddinger R, Saleh A, Shun T, Vernetti LA, Gough A. A 3D microfluidic liver model for high throughput compound toxicity screening in the OrganoPlate(R). Toxicology. 2021;450:152667. https://doi.org/10.1016/j.tox.2020.152667.

44. Brooks A, Liang X, Zhang Y, Zhao CX, Roberts MS, Wang H, Zhang L, Crawford DHG. Liver organoid as a 3D in vitro model for drug validation and toxicity assessment. Pharmacol Res. 2021;169:105608. https://doi.org/10.1016/j.phrs.2021.105608.

45. Ewart L, Apostolou A, Briggs SA, Carman CV, Chaff JT, Heng AR, Jadalannagari S, Janardhanan J, Jang KJ, Joshipura SR, et al. Performance assessment and economic analysis of a human

Liver-Chip for predictive toxicology. Commun Med (Lond). 2022;2:154. https://doi.org/10.1038/s43856-022-00209-1.

46. Harrison SP, Baumgarten SF, Verma R, Lunov O, Dejneka A, Sullivan GJ. Liver organoids: recent developments, limitations and potential. Front Med (Lausanne). 2021;8:574047. https://doi.org/10.3389/fmed.2021.574047.

47. Nuciforo S, Fofana I, Matter MS, Blumer T, Calabrese D, Boldanova T, Piscuoglio S, Wieland S, Ringnalda F, Schwank G, et al. Organoid models of human liver cancers derived from tumor needle biopsies. Cell Rep. 2018;24:1363–76. https://doi.org/10.1016/j.celrep.2018.07.001.

48. Valdoz JC, Johnson BC, Jacobs DJ, Franks NA, Dodson EL, Sanders C, Cribbs CG, Van Ry PM. The ECM: to scaffold, or not to scaffold, that is the question. Int J Mol Sci. 2021;22 https://doi.org/10.3390/ijms222312690.

49. Li X, Tang J, Mao Y. Incidence and risk factors of drug-induced liver injury. Liver Int. 2022;42:1999–2014. https://doi.org/10.1111/liv.15262.

50. Anderson GD. Sex and racial differences in pharmacological response: where is the evidence? Pharmacogenetics, pharmacokinetics, and pharmacodynamics. J Womens Health (Larchmt). 2005;14:19–29. https://doi.org/10.1089/jwh.2005.14.19.

51. Sayaf K, Gabbia D, Russo FP, De Martin S. The role of sex in acute and chronic liver damage. Int J Mol Sci. 2022;23 https://doi.org/10.3390/ijms231810654.

52. Soldin OP, Mattison DR. Sex differences in pharmacokinetics and pharmacodynamics. Clin Pharmacokinet. 2009;48:143–57. https://doi.org/10.2165/00003088-200948030-00001.

53. Sipes NS et al. An intuitive approach for predicting potential human health risk with the tox21 10k library. Environ Sci Technol 2017;51(18):10786–96.

54. Lurvink RJ, et al. Systemic Pharmacokinetics of Oxaliplatin After Intraperitoneal Administration by Electrostatic Pressurized Intraperitoneal Aerosol Chemotherapy (ePIPAC) in Patients with Unresectable Colorectal Peritoneal Metastases in the CRC-PIPAC Trial. Ann Surg Oncol 2021;28(1): 265–72.

55. Ikeda M, et al. Safety and Pharmacokinetics of Lenvatinib in Patients with Advanced Hepatocellular Carcinoma. Clin Cancer Res 2016;22(6):1385–94.

56. Jones R, et al. Quantitation of Cabozantinib in Human Plasma by LC-MS/MS. J Chromatogr Sci 2022;60(3):274–9.

57. Brendel E, et al. Pharmacokinetic results of a phase I trial of sorafenib in combination with dacarbazine in patients with advanced solid tumors. Cancer Chemother Pharmacol 2011;68(1):53–61.